Petroleum Science 20 (2023) 3119–3130

Contents lists available at ScienceDirect

Petroleum Science

journal homepage: www.keaipublishing.com/en/journals/petroleum-science

Original Paper

Effect of hydraulic fracturing induced stress field on weak surface activation during unconventional reservoir development

Jie Bai [a, b], Xiao-Qiong Wang [a, b, *], Hong-Kui Ge [a, b], Hu Meng [a, b], Ye-Qun Wen [a, b]

[a] Unconventional Petroleum Research Institute, China University of Petroleum (Beijing), Beijing, 102249, China
[b] State Key Laboratory of Petroleum Resources and Engineering, China University of Petroleum (Beijing), Beijing, 102249, China

ARTICLE INFO

Article history:
Received 27 September 2022
Received in revised form
31 December 2022
Accepted 6 May 2023
Available online 6 May 2023

Edited by Jia-Jia Fei

Keywords:
Hydraulic fracturing
Induced stress field
Weak surface
Natural fracture stability
Fracturing characteristics

ABSTRACT

Unconventional reservoirs usually contain many weak surfaces such as faults, laminae and natural fractures, and effective activation and utilization of these weak surfaces in reservoirs can significantly improve the extraction effect. In hydraulic fracturing, when the artificial fracture approaches the natural fracture, the natural fracture would be influenced by both the original *in-situ* stress field and the hydraulic fracturing-induced stress field. In this paper, the hydraulic fracturing-induced stress field is calculated based on the relative position of hydraulic fracture and natural fracture, the original *in-situ* stress, the net pressure inside the hydraulic fracture and the pore pressure of the formation. Furthermore, the stability model of the natural fracture is established by combining the Mohr-Coulomb rupture criterion, and extensive parametric studies are conducted to explore the impact of each parameter on the stability of the natural fracture. The validity of the proposed model is verified by comparing with the reservoir characteristics and fracturing process of the X-well 150–155 formation in the Songliao Basin. It is found that the stress field induced by the hydraulic fracture inhibits the activation of the natural fracture after the artificial fracture crossed the natural fracture. Therefore, for similar reservoirs as X-well 150–155, it is suggested to connect natural fractures with hydraulic fractures first and then activate natural fractures which can effectively utilize the natural fractures and form a complex fracture network.

1. Introduction

Since the 13th Five-Year Plan, China's new proven oil and gas reserves are mainly unconventional oil and gas resources (Lei et al., 2022a, b). Large-scale hydraulic fracturing is a key technology for the efficient development of unconventional oil and gas reservoirs (Wang et al., 2020; Lu et al., 2021; Zhao et al., 2020). Unconventional reservoirs contain many weak surfaces such as faults, laminae and natural fractures. As shown in Fig. 1, obvious laminae development can be seen in the reservoir cores of unconventional oil and gas producing areas in China such as the Qingshankou Formation in the southern part of the Songliao Basin, the Ganchaigou Formation in the Tsaidam Basin and the Longmaxi Formation in the Sichuan Basin. These laminae and natural fractures play an important role in the formation of fracture network induced by hydraulic (Wang et al., 2018, 2021; Yildirim et al., 2018). Fracturing tests in mines have shown that geological discontinuities such as joints and faults in the formation may be preferentially activated and interconnected, which in turn affects the propagation of hydraulic fractures (Warpinski and Teufel, 1987). Microseismic monitoring results show that some of the natural fractures will open and slip when the artificial fractures approach them (Maxwell, 2011). Indoor true triaxial hydraulic fracturing experiments of shale have also demonstrated that the interaction between hydraulic fractures and weak surfaces can form a very complex fracture morphology (Liu et al., 2019; Tan et al., 2020). Under the condition where there is little difference between vertical stress and minimum horizontal principal stress, the laminae are easily opened by hydraulic fractures, which will result in a single horizontal fracture. Therefore, maintaining an appropriate stress difference during hydraulic fracturing facilitates the formation of a fracture network (Zou et al., 2022; Chi et al., 2018; Tan et al., 2017). The interfacial friction coefficient is one of the important factors for hydraulic fractures to pass through natural fractures, and mutual misalignment or tip blunting between

* Corresponding author. State Key Laboratory of Petroleum Resources and Prospecting, China University of Petroleum, (Beijing), Beijing, 102249, China.
E-mail address: wxq4526@163.com (X.-Q. Wang).

https://doi.org/10.1016/j.petsci.2023.05.003

Fig. 1. Unconventional oil and gas reservoir core. (**a**) Core of Qingshankou Formation, southern Songliao Basin; (**b**) Core of Longmaxi Formation in Weiyuan, Sichuan Basin; (**c**) Core of Ganchaigou Formation in Yingxiongling, Qaidam Basin.

natural fracture surfaces can lead to the termination, extension or changing of propagation direction of hydraulic fractures (Bunger et al., 2015; Altammar et al., 2017). Therefore, in the process of unconventional oil and gas development, effective activation of natural weak surfaces is conducive to the formation of complex fracture networks, which in turn improves the efficiency of hydraulic fracture modification. Under the original *in-situ* stress state, the natural fractures within the reservoir are in a stable state (Yang et al., 2020a, b; Gong et al., 2021). During the hydraulic fracturing process, the artificial fracture will change the stress state around the fracture when it propagates and approaches the natural fracture. Due to this disturbance, the natural fracture will subject to tension and shear failure, which is called the unstable state. In the hydraulic fracturing process, the approach distance and approach angle between the hydraulic fracture and the natural fracture, as well as the difference in original main *in-situ* stress, the stress difference coefficient, the net pressure within the hydraulic fracture, the pore pressure of formation, the length of the hydraulic fracture and other factors will all have an impact on the stability of the natural fracture (Chuprakov and Zhubayev, 2010; Zou et al., 2016; Blanton, 1986; Zhao et al., 2021; Teufel and Clark, 1984; Lei et al., 2021; Zhang et al., 2018; Weng and Siebrits, 2007). The activation of natural fractures is positively correlated with the angle between the hydraulic fracture and the natural fracture. Therefore, it is easier for the hydraulic fracture to propagate and to cross the natural fracture with a larger angle between the hydraulic fracture and the natural fracture (Tang et al., 2018). Low-strength laminae tend to trap hydraulic fractures, while high-strength laminae are easily crossed by hydraulic fractures. However, weak laminae can also be crossed by the hydraulic fractures by adjusting the fracturing process (Lei et al., 2022a, b; Huang et al., 2022). Dong et al. (2019) determined whether shear slip could occur in natural fractures based on the Mohr-Coulomb criterion and found that most natural fractures and faults would be activated under high net pressure. Zhang et al. (2015) developed a theoretical model for predicting fracture propagation in tight oil reservoirs and investigated the effects of difference in horizontal stress, number of shot hole clusters, shot hole cluster spacing, injection rate and natural fracture linear density on fracture propagation. Guo et al. (2014) found that under simulated triaxial stress conditions, hydraulic fracturing can produce fractures that are perpendicular to the laminar surface, which will then intersect with the fractures formed after the laminar surface is cracked and form a fracture network. Tan et al. (2021) proposed the notion of transition zone in layered formation and studied the effect of multiple influencing factors on hydraulic fracture propagation behavior based on FEM-based CZM method. The obtained results were conformed to the experimental observation (Tan et al., 2019).

Current research on natural fracture stability focus more on the initial stress condition of the reservoir, while less attentions are given to the impact of the presence of hydraulic fractures on natural fractures. The initiation and propagation of hydraulic fractures can induce stresses that change the magnitude and direction of the *in-situ* stress around the fracture, which together with the original *in-situ* stress field have an impact on natural fracture stability. Hydraulic fractures can pass through natural fractures directly without changing direction, or they can be interrupted or bifurcated along natural fractures (Warpinski and Teufel, 1987; Jeffrey and Weber, 1994). Sneddon (1946) proposed an analytical expression for the stress field around fractures in infinite elastomers, stating that the induced stress in the direction of the minimum principal stress is greater than that in the direction of the maximum principal stress. Li et al. (2014) developed an analytical model based on infinitely large homogeneous rocks for predicting fracture-induced stress fields, which provided a basis for modelling fracture extension. The presence of induced stresses at the tip of a hydraulic fracture can make natural fractures open or extend (Olson and Arash, 2009). Methods to calculate the fracturing induced stress field include the discrete element method and the extended finite element method, in which the induced stress field from fracturing and stress disturbance between fractures can be simulated (Shimizu et al., 2011; Meng et al., 2021). During the extraction of unconventional oil and gas reservoirs, in order to fully activate the natural weak surface, techniques such as temporary plugging and repetitive fracturing can be used to increase the reformation volume (Zheng et al., 2022).

The abovementioned researches on induced stress fields are all based on the situation where the hydraulic fractures do not contact the natural fractures. However, in the Songliao Basin Well X reservoir, where the natural fractures are orthogonal to the direction of the maximum principal stress, a fracturing scheme where the hydraulic fractures firstly pass through multiple natural fractures before activating the natural fractures is adopted. In this circumstance, the influence of the induced stress field generated on

the stability of the natural fractures needs to be considered when the hydraulic fracture crosses the natural fractures. This paper calculated the induced stress field of hydraulic fractures based on the linear elastic fracture mechanics theory and established a stability model of natural fracture based on the Mohr-Coulomb criterion. The model is validated by comparing with the field data. Extensive parametric studies are conducted to investigate the activation characteristics of hydraulic fractures approaching and crossing natural fractures. Corresponding suggestions are given for optimizing borehole trajectories and hydraulic fracturing schemes for similar reservoirs.

2. Theoretical model

2.1. Weak surface activation mechanical model

To facilitate the study, the natural weak surface was simulated by a two-dimensional model with the force state shown in Fig. 2. Its slip characteristics are governed by the Mohr-Coulomb criterion. In the σ-τ plane, the rock fracture line and Mohr circle are shown in Fig. 3. The Mohr circle is determined by the maximum and minimum effective principal stresses σ_1 and σ_3, and the diameter is the difference in principal stresses.

$$\tau = C + \sigma \tan \varphi \tag{1}$$

in which C is the intercept of rock fracture line and τ axis, i.e., the cohesion of rock; φ is the internal friction angle of rock.

The relative position of the rupture line and the Mohr circle can be used to determine whether a rupture has occurred or not. When the Mohr circle drawn according to the *in-situ* stress is not in contact with the rock rupture line, no rupture occurs, i.e., the rock is in a stable state; when the Mohr circle is tangent to the rupture line, then an equilibrium state is reached, where the shear stress reaches the shear strength at a certain angle. There is also a state where the Mohr circle intersects the rupture line geometrically, but in fact, the rock has been destroyed before the intersected state.

For intact rock, fracture is the only mechanism of failure, which is governed by the Mohr-Coulomb criterion (Chen et al., 2021). For the strata with weak surface such as faults and weak surface interlayers, the failure mode can be both the fracture through the discontinuities and the sliding along the discontinuities (Zoback and Snee, 2018). In general, the shear strength of the weak surface is lower than the strength of the rock matrix. Assuming that the cohesion on the discontinuity surface is 0, the fracture line of the weak surface can be drawn as shown in Fig. 4.

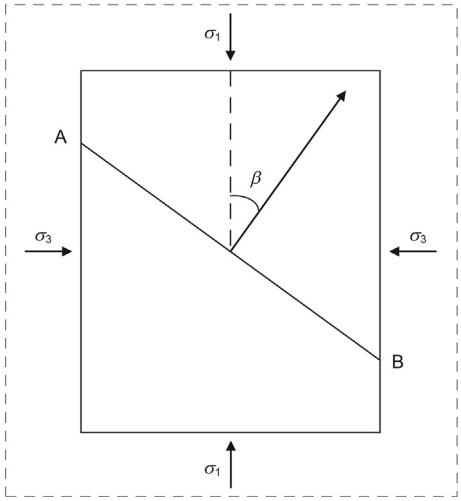

Fig. 2. Relationship between weak plane and principal stress. (Among them, σ_1 and σ_3 are the maximum and minimum effective stresses of strata; AB is the discontinuity surface; β is the angle between normal direction of discontinuity and maximum principal stress).

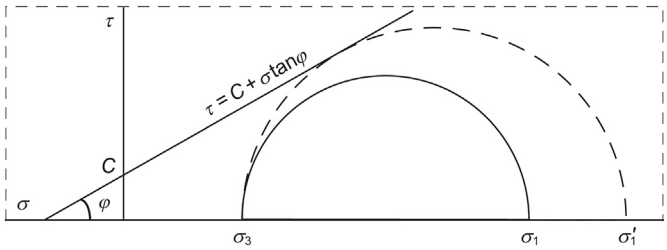

Fig. 3. Mohr-Coulomb criterion.

In the σ-τ plane, the rupture line of the rock matrix is represented by line A and the rupture line of the weak surface of the rock is represented by line B. Points L and M are the two intersections of the line B with the Mohr circle. Note that the angle normal to the direction of maximum principal stress in the weak side is β (Fig. 2). The angle between any radius on the Mohr circle and the positive direction of the σ axis is 2β.

In circle O_3, the Mohr circle is not in contact with the B line, which indicates that the formation is in a stable state and neither rock fracture nor sliding along the weak surface occurs. Assuming a constant minimum principal stress σ_3 and an increasing maximum principal stress σ_1, the Mohr circle expands gradually until it is tangential to the line B. Further increase of σ_1 will lead to the intersection of Mohr circle and line B. When $2\beta_1 < 2\beta < 2\beta_2$, sliding along the weak face occurs; when $2\beta < 2\beta_1$ or $2\beta > 2\beta_2$, the rock is in a stable state, no rupture occurs, and no sliding along the weak face occurs. When the maximum principal stress continues to increase and the Mohr circle is tangent to the A line, reaching the circle O_1 state shown, the rock mass itself is in ultimate equilibrium and there is a possibility of damage.

In conclusion, the strata will slip after the Mohr circle intersects the weak surface rupture line only if 2β falls in a specific range. Otherwise, no slip along the weak surface will occur even if the formation itself is damaged.

During hydraulic fracturing, when fluid enters the weak surface of the formation, its initial stress state will be changed. As the fluid entering the weak surface (hereafter, weak surface is replaced with natural fracture), the pore pressure increases and the effective principal stress acted on the weak surface decreases. As a consequence the Mohr circle moves leftwards in the "σ-τ" coordinate system as shown in Fig. 5.

During the movement of the Mohr circle from the O to the O', its secant with the fracture line changes from the LM to the $L'M'$ and the angular range of possible shear slip increases. This principle is often applied to the activation of natural fractures in

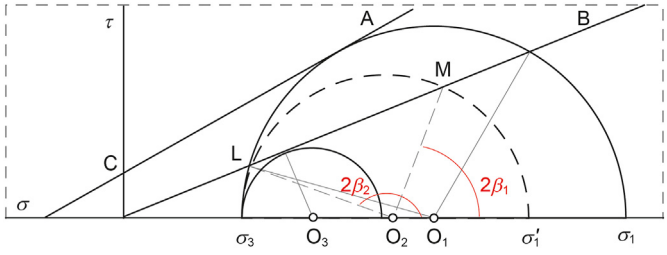

Fig. 4. Mohr-Coulomb criterion with weak surface.

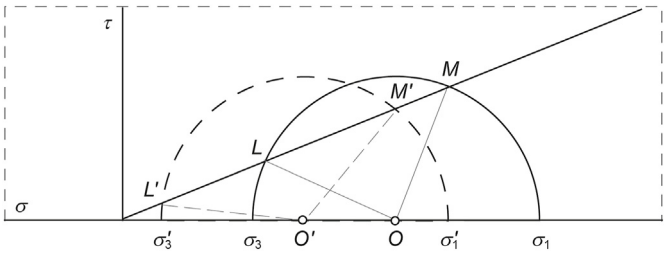

Fig. 5. Change in stress state at interrupted surface with change in pore pressure.

unconventional oil and gas extraction to create complex fracture networks and improve fracturing efficiency (Sesetty and Ahmad, 2019).

2.2. Hydraulic fracture-induced stress field model

The natural fractures in reservoirs are basically in a stable state under the original *in-situ* stress. In contrast, during hydraulic fracturing, when the hydraulic fracture approaches the natural fracture, fracturing induced stress will be generated, and the natural fracture may become unstable under the combined effect of original *in-situ* stress and the induced stress.

The stress field is calculated analytically based on the theory of complex functions (Yew and Weng, 2015; Yang et al., 2021). The stress field at point A in Fig. 6 can be expressed as

$$\sigma_z = (\sigma_h - p)\cdot f^+ + \sigma_h \tag{2}$$

$$\sigma_x = (\sigma_h - p)\cdot f^- + \sigma_H \tag{3}$$

$$\tau_{zx} = (\sigma_h - p)\frac{a^2 r \sin\theta \cos\left[\frac{3}{2}(\theta_1+\theta_2)\right]}{\sqrt{(r_1 r_2)^3}} \tag{4}$$

$$\sigma_y = \upsilon(\sigma_x + \sigma_z) \tag{5}$$

where σ_h and σ_H represent the minimum and maximum horizontal principal stresses in the far field, respectively; a is the half-length of hydraulic fracture; p is the fluid pressure in the fracture; and υ is the rock Poisson's ratio; f^+ and f^- are two abbreviations, the detailed expression of which are given ass:

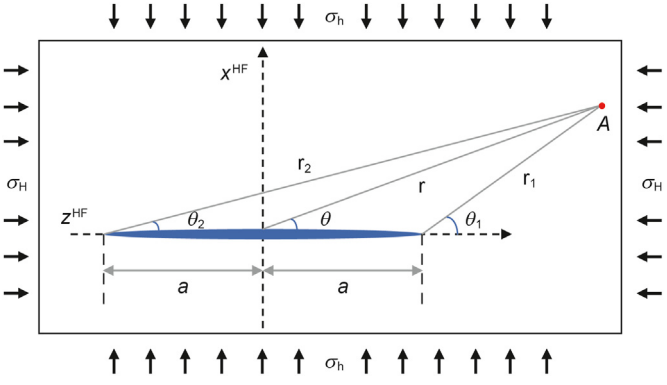

Fig. 6. The schematic diagram of the stress induced by a hydraulic fracture.

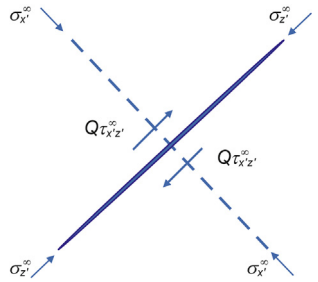

Fig. 7. The schematic diagram of natural fracture stress field.

$$f^+ = \frac{r}{\sqrt{r_1 r_2}}\cos\left(\theta - \frac{\theta_1+\theta_2}{2}\right) + \frac{a^2 r}{\sqrt{(r_1 r_2)^3}}\sin\theta\sin\left[\frac{3}{2}(\theta_1+\theta_2)\right] - 1 \tag{6}$$

$$f^- = \frac{r}{\sqrt{r_1 r_2}}\cos\left(\theta - \frac{\theta_1+\theta_2}{2}\right) - \frac{a^2 r}{\sqrt{(r_1 r_2)^3}}\sin\theta\sin\left[\frac{3}{2}(\theta_1+\theta_2)\right] - 1 \tag{7}$$

$$\begin{cases} \theta = \arctan\left(\dfrac{x}{z}\right) \\ \theta_1 = \arctan\left(\dfrac{x}{z-a}\right) \\ \theta_2 = \arctan\left(\dfrac{x}{z+a}\right) \end{cases} \tag{8}$$

$$\begin{cases} r = \sqrt{x^2+z^2} \\ r_1 = \sqrt{x^2+(z-a)z^2} \\ r_2 = \sqrt{x^2+(z+a)z^2} \end{cases} \tag{9}$$

As indicated by Eqs. (2) and (3), the stress field is obtained by adding the fracturing induced stress to the original *in-situ* stress. The net pressure is negative in the calculation of the induced stress, meaning that the hydraulic fracturing induced stress is the tensile stress within a certain range.

The hydraulically fracture-induced stress field is modelled as:

$$\Delta\sigma_z = (\sigma_h - p)\cdot f^+ \tag{10}$$

$$\Delta\sigma_x = (\sigma_h - p)\cdot f^- \tag{11}$$

$$\Delta\tau_{zx} = (\sigma_h - p)\frac{a^2 r \sin\theta \cos\left[\frac{3}{2}(\theta_1+\theta_2)\right]}{\sqrt{(r_1 r_2)^3}} \tag{12}$$

$$\sigma_y = \upsilon(\sigma_x + \sigma_z) \tag{13}$$

2.3. Natural fracture stress field

The activation of natural fractures can be influenced by the roughness of their surface. The analysis of the natural fracture stress field requires consideration of the roughness of the fracture

surface. In addition, natural fractures in the reservoir do not develop exactly in the direction of the maximum principal stress due to factors such as the burial depth, *in-situ* stress, matrix strength and mineral fraction. Assuming a natural fracture half-slit length of h, the analysis is carried out for the *x-z* plane as shown in Fig. 7.

Stress field of natural fracture can be obtained as (Dyer, 1988):

$$\begin{cases} \tau_{x'z'} = (1-Q)\left[\tau^{\infty}_{x'z'}\dfrac{x}{\sqrt{x^2+h^2}}\right] + Q\tau^{\infty}_{x'z'} \\ \sigma_{x'} = \sigma^{\infty}_{x'} \\ \sigma_{z'} = \sigma^{\infty}_{z'} \end{cases} \tag{14}$$

where Q denotes the degree of natural fracture closure and takes the value range 0–1; $\sigma^{\infty}_{x'}$, $\sigma^{\infty}_{z'}$ and $\tau^{\infty}_{x'}$ denote the original stresses and tangential stresses perpendicular to, and along, the natural fracture direction, respectively, which can be obtained from the two-dimensional stress solution.

2.4. Hydraulic fractures approaching natural fractures

As demonstrated from above formulations, the stress field around a hydraulic fracture (HF) or a natural fracture (NF) is affected by various factors such as the original *in-situ* stress and the orientation of the fracture, and the induced stresses in the process of approaching the natural fracture can affect the stability of the natural fracture.

As shown in Fig. 8, the approach angle between the hydraulic fracture and the natural fracture (the angle between the natural fracture and the maximum horizontal principal stress) is α, and the distance between the front of HF and NF is *L*. The plane of $y^{NF} = y^{HF} = 0$ is taken for analysis.

From Eq. (10)–(12), the magnitude and direction of the principal stress at point A for the hydraulic fracture induced stress can be calculated. The induced stress generated by the hydraulic fracture at point A can be transformed into a local principal stress by the following equations:

$$\begin{cases} \Delta\sigma_1 = \dfrac{\Delta\sigma_x + \Delta\sigma_z}{2} + \sqrt{\Delta\tau_{xz}^2 + \left(\dfrac{\Delta\sigma_z - \Delta\sigma_x}{2}\right)^2} \\ \Delta\sigma_3 = \dfrac{\Delta\sigma_x + \Delta\sigma_z}{2} - \sqrt{\Delta\tau_{xz}^2 + \left(\dfrac{\Delta\sigma_z - \Delta\sigma_x}{2}\right)^2} \\ \varphi = \sin^{-1}\left[\dfrac{-\Delta\tau_{xz}}{\sqrt{(\Delta\sigma_x - \Delta\sigma_3)^2 + \Delta\tau_{xz}^2}}\right] \end{cases} \tag{15}$$

The induced principal stresses generated by HF at point A can be converted to stresses at NF by the following equation, as shown in Fig. 9.

$$\begin{cases} \Delta\sigma_x^{HF} = \dfrac{\Delta\sigma_1 + \Delta\sigma_3}{2} - \dfrac{\Delta\sigma_1 - \Delta\sigma_3}{2}\cos 2(\alpha - \varphi) \\ \Delta\sigma_z^{HF} = \dfrac{\Delta\sigma_1 + \Delta\sigma_3}{2} + \dfrac{\Delta\sigma_1 - \Delta\sigma_3}{2}\cos 2(\alpha - \varphi) \\ \Delta\tau_{xz}^{HF} = -\dfrac{\Delta\sigma_1 - \Delta\sigma_3}{2}\sin 2(\alpha - \varphi) \end{cases} \tag{16}$$

Superimposing the induced stress at the natural fracture face (Eq. (16)) and the original *in-situ* stress (Eq. (14)), the stress field at the natural fracture is obtained as :

$$\begin{cases} \sigma_x^{HF} = \sigma_x^{\infty} + \Delta\sigma_x^{HF} \\ = \dfrac{\sigma_H^{\infty} + \Delta\sigma_1 + \sigma_h^{\infty} + \Delta\sigma_3}{2} - \dfrac{\sigma_H^{\infty} - \sigma_h^{\infty}}{2}\cos 2\alpha - \dfrac{\Delta\sigma_1 - \Delta\sigma_3}{2}\cos 2(\alpha - \varphi) \\ \sigma_z^{HF} = \sigma_z^{\infty} + \Delta\sigma_z^{HF} \\ = \dfrac{\sigma_H^{\infty} + \Delta\sigma_1 + \sigma_h^{\infty} + \Delta\sigma_3}{2} + \dfrac{\sigma_H^{\infty} - \sigma_h^{\infty}}{2}\cos 2\alpha + \dfrac{\Delta\sigma_1 - \Delta\sigma_3}{2}\cos 2(\alpha - \varphi) \\ \tau_{xz}^{HF} = -Q\dfrac{\sigma_H^{\infty} - \sigma_h^{\infty}}{2}\sin 2\alpha - \dfrac{\Delta\sigma_1 - \Delta\sigma_3}{2}\sin 2(\alpha - \varphi) \end{cases} \tag{17}$$

According to the Mohr-Coulomb criterion, the condition for occurrence of shear instability in natural cracks is

$$\left|\tau_{xz}^{HF}\right| > \tau_0 + K_f\left(\sigma_x^{HF} - p_p\right) \tag{18}$$

The condition for occurrence of tension instability is that the pore pressure in the seam is greater than the sum of the positive stress and the tensile strength at the face of natural fracture. With the tensile strength at the seam face taken as 0, the condition can expressed as

$$p_p - \sigma_x^{HF} > 0 \tag{19}$$

where K_f is the friction coefficient of the inner surface of natural fracture; p_p is the formation pore pressure; and τ_0 is the inherent shear strength of natural fracture.

The parameters taken as initial values of the model for stability

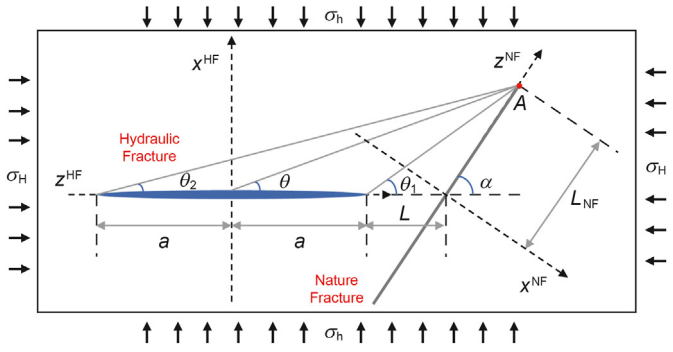

Fig. 8. Hydraulic fracture approaching natural fracture diagram.

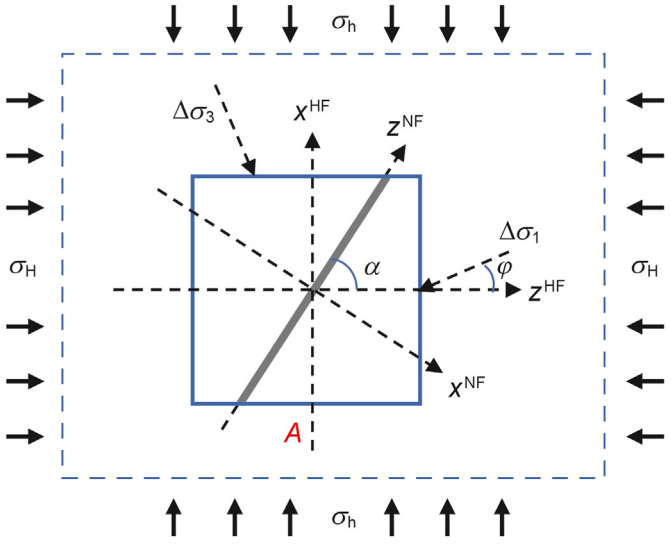

Fig. 9. Amplified diagram of the induced stress in the hydraulic fracture at point A.

analysis is summarized in Table 1. The approach distance indicates the distance between the hydraulic fracture and the natural fracture in the direction of its development. The angle of approach indicates the angle between the hydraulic fracture and the natural fracture. The net pressure represents the difference between the fluid in the hydraulic fracture and the minimum principal stress.

With the above parameters, a schematic representation of the natural fracture stability is depicted in Fig. 10. In the diagram, "Distance from center" indicates the distance between the point on the natural fracture with the intersection of the hydraulic fracture and the natural fracture. For shear stability, Natural fracture stability is denoted $|\tau_{xz}^{HF}| - [\tau_0 - K_f(\sigma_x^{HF} - p_p)]$; for tension stability, Natural fracture stability is denoted $p_p - \sigma_x^{HF}$. It can be found that the natural fractures appear to be and are susceptible to shear slip without tension damage.

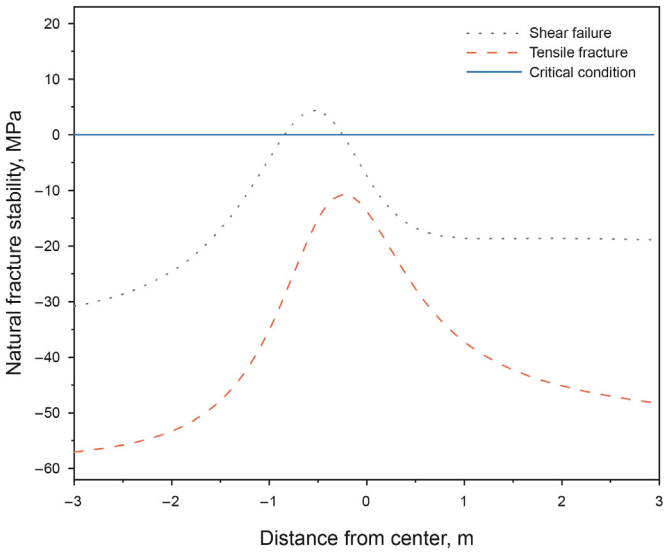

Fig. 10. Natural fracture stability analysis.

3. Results and discussion

The sensitivity analysis of different factors was carried out to explore their influence on the stability of natural fractures. One of the variables is changed during the sensitivity analysis, while other parameters are kept constants as given in Table 1.

3.1. Effect of approach distance on stability of natural fracture

The approach distance indicates the distance between the hydraulic fracture and the natural fracture in the direction of its development. Adjusting the approach distance and keeping the other parameter values constant, the shear stability and tension stability of the natural fracture with different approaching distance is plotted in Fig. 11(a) and (b), respectively. As the approach distance decreases from 1.5 to 1 m, shear instability begins to occur in natural fracture. When the approach distance further decreased to 0.6 m, the natural fracture shows both shear and tension instability.

Therefore, as the approach distance decreases, the natural fractures are gradually affected by the induced stress field. At the same approach distance, shear damage is more likely to occur in natural fractures than tension damage. With the adopted parameters, the critical approach distance for shear instability is around 1.2 m.

3.2. Influence of the angle of approach on the stability of natural fractures

The angle of approach refers to the angle between the direction of hydraulic fracture extension and the natural fracture. Adjusting the approach angle and keeping the other parameter values constant, shear stability and tension stability of the natural fracture with different approach angles are depicted in Fig. 12. As the approach angle decreases from 90° to 70°, the shear instability of natural fracture appears. As for the tension instability of natural fracture, when the approach angle decreases to 50°, it begin to occur.

It can be demonstrated that natural fractures tend to stabilize when the angle of approach is large. It can also be concluded that natural fractures are more susceptible to shear damage and tensile damage is less likely to occur than shear damage, which conforms to the trend in Section 2.1.

3.3. Effect of net pressure on the stability of natural fractures

Observation of Fig. 13 reveals that the net pressure within the hydraulic fracture has a significant effect on the stability of the natural fracture, and a variation of just 1 MPa net pressure has the potential to destabilize the natural fracture. By adopting different net pressures, it can be found that when the net pressure increases from 5 to 7 MPa, the natural fracture gradually becomes shear destabilized. And shear instability occurs when the net pressure reaches 6 MPa. As the net pressure continues to increase to 9 MPa, the natural fractures appear to be unstable in tension. As the net pressure increases, the induced stress field will induce instability of a larger and larger area of. Also, shear instability is more likely to occur than tension instability.

3.4. Effect of formation pore pressure on the stability of natural fractures

The effect of formation pore pressure on the stability of natural fractures is shown in Fig. 14. The stability of natural fractures decreases with the increase of formation pore pressure. It is known from the Mohr-Coulomb rock rupture criterion that the effective stress in the rupture criterion decreases with the increase of pore pressure, which increases the probability for shear rupture to occur. Therefore, when other conditions are the same, the higher the formation pore pressure is, the more unstable the natural fractures

Table 1
Parameter values of influence factors of induced stress field.

Influencing factors	Parameter values	Influencing factors	Parameter values
Maximum horizontal principal stress	118 MPa	Minimum horizontal principal stress	106 MPa
Vertical principal stress	132 MPa	Poisson ratio	0.2
Inherent shear strength of natural fractures	4 MPa	Pore pressure	60 MPa
Degree of natural fracture closure	0.9	Hydraulic fracture half slit length	100 m
Friction coefficient in natural fracture	0.5	Net pressure	7 MPa
Approach angle	70°	Approach distance	1 m

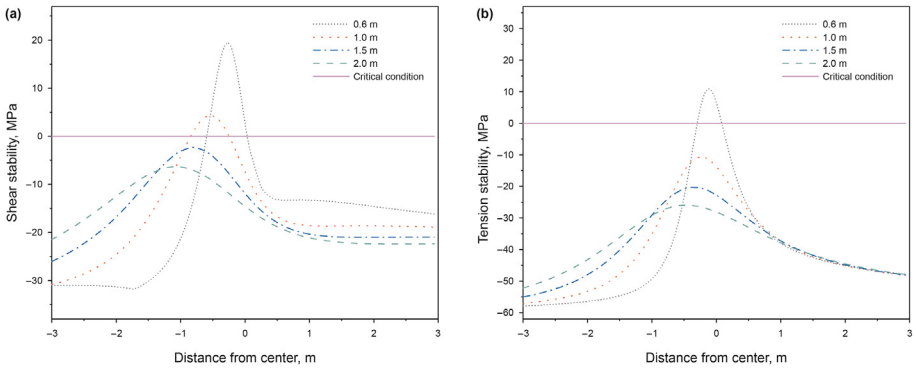

Fig. 11. (**a**) Effect of approach distance on shear stability of natural fractures; (**b**) Effect of approach distance on the tension stability of natural fractures.

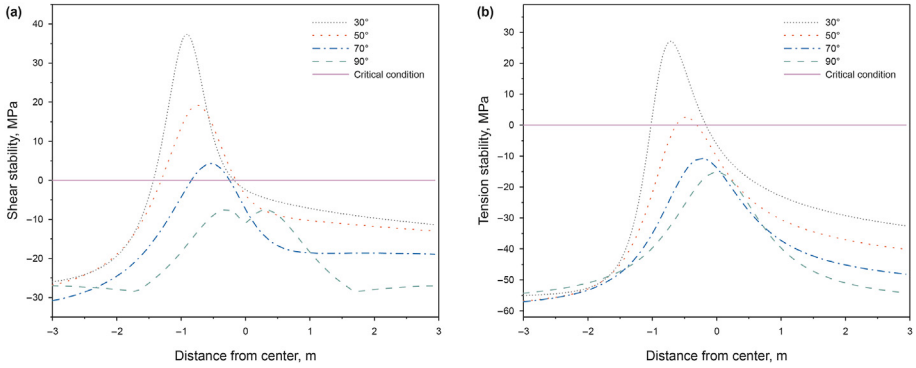

Fig. 12. (**a**) Effect of approach angle on shear stability of natural fractures; (**b**) Effect of approach angle on the tension stability of natural fractures.

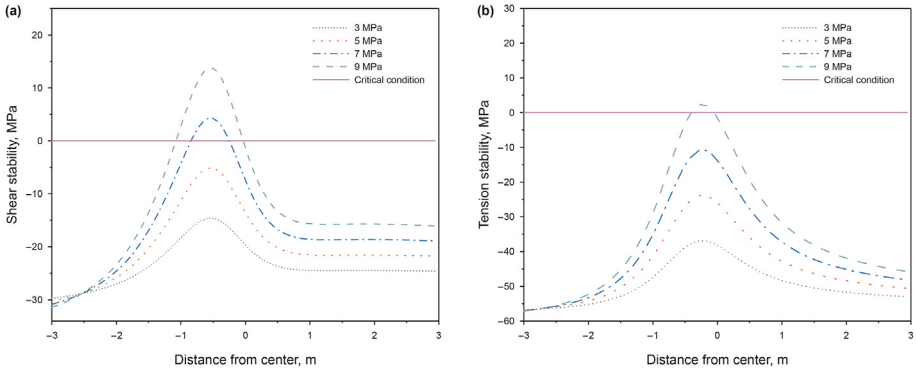

Fig. 13. (**a**) Effect of net pressure on the shear stability of natural fractures; (**b**) Effect of net pressure on the tension stability of natural fractures.

are. The area of instability increases with the increase of pore pressure.

3.5. Effect of horizontal stress differences on the stability of natural fractures

When analyzing the effect of differential horizontal stress on the stability of natural fractures, both maximum and minimum principal stresses are adjusted so that the coefficient horizontal stress discrepancy factor, as defined in Eq. (19), remains constant, while keeping the parameters constant.

$$K = \frac{\sigma_H - \sigma_h}{\sigma_h} \tag{19}$$

The results shows that, with a constant horizontal stress discrepancy factor and keeping a certain net pressure in the seam, the stability of the natural fracture increases continuously with the increase of the horizontal principal stress difference. As the horizontal stress difference decreases from 13 to 12 MPa, shear instability of natural fracture develops. Therefore, the effect of the horizontal principal stress difference on the stability of the natural fracture is very significant.

3.6. Effect of horizontal stress discrepancy factor on the stability of natural fractures

In Fig. 16, both the maximum and minimum principal stresses are adjusted to keep the horizontal stress difference constant while changing the horizontal stress discrepancy factor.

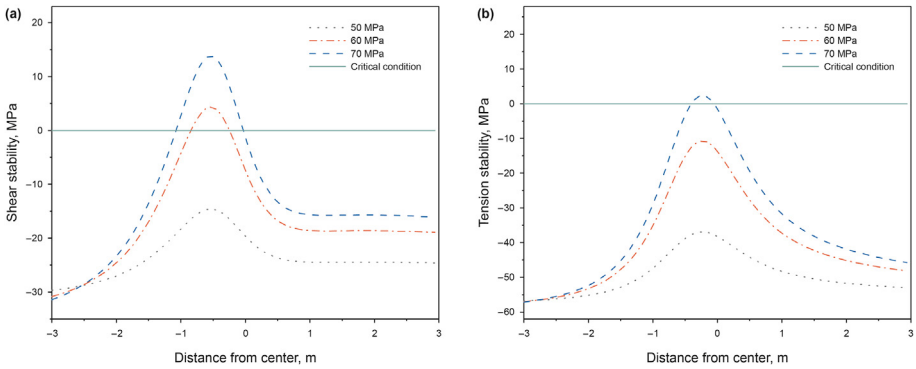

Fig. 14. (**a**) Effect of formation pore pressure on the shear stability of natural fractures; (**b**) Effect of pore pressure on tensile stability of natural fractures.

From Fig. 16, it indicates that when the horizontal stress difference and the net pressure inside the seam are certain, the stability of natural fracture decreases with the increase of the horizontal stress difference coefficient. When the natural fracture is destabilized, the shear rupture area decreases with the decrease of the horizontal stress difference coefficient. From Figs. 15 and 16, it shows that the stability of natural fractures is not only affected by the horizontal stress difference, but also by the horizontal stress difference coefficient, and the horizontal stress difference coefficient has a significant influence on the stability of natural fractures.

3.7. Effect of half length of hydraulic fracture on natural fracture stability

As seen from Fig. 17, the stability of natural fractures increases as the length of the hydraulic fracture decreases. This can be attributed to the fact that the longer the hydraulic fracture is, the greater the range of influence of the induced stress it produces. However, it is interesting to find that the change in the length of the hydraulic fracture does not affect the location of the instability.

4. Case study

Nowadays, the Changling Block in the Songliao Basin is being studied for the development of deep tight gas. According to the logging data and physical analysis, the natural fractures in the Shahezi Formation reservoir of Well X are moderately developed and oriented mainly in a north-south direction, orthogonal to the direction of the maximum principal stress. The target reservoir is deeply buried with a large *in-situ* stress is large, and the stress difference between the two directions is around 12 MPa, which requires relatively high pressure for fracturing construction and makes construction difficult.

Table 2 summarizes the basic properties of fractures around the well obtained by geophysical prospecting in layer No.150-155 of X well. At the depth of 5390–5440 m, natural fractures are mainly distributed in 30° azimuth and 0° azimuth. In hydraulic fracturing, hydraulic fractures extend along the direction of maximum principal stress (east-west direction). Therefore, it is assumed that the angle between hydraulic fracture and natural fracture (approaching angle) is 60° or 90°, and the stability of natural fracture is analyzed according to the parameters given in Table 3.

Table 3 shows the basic parameters of the studied layers, which are substituted into the stability model to obtain the stability of the natural fractures in the target layer.

According to Figs. 18 and 19, it can be found that at the target layer, for fractures with azimuths of 30° and 0°, the natural fractures can be activated to shear slip when the net pressure of the hydraulic fractures reaches 9.3 and 16.5 MPa (see Fig. 20).

The positive hydraulic fracture stress is the net pressure in the fracture plus the minimum principal stress, and the wellhead pumping pressure is the positive hydraulic fracture stress minus the formation pore pressure. The positive hydraulic fracture stress in this example is 126.5 MPa (110+16.5 = 126.5 MPa, the minimum principal stress plus the net pressure). The wellhead pumping pressure has to reach 60.5 MPa (126.5−66 = 60.5 MPa, the positive hydraulic fracture stress minus the pore pressure) to activate the fractures at 30° and 0°.

In the above model, it is assumed that the hydraulic fracture activates the natural fracture when the hydraulic fracture approaches the natural fracture at a distance of 1.5 m and the net pressure in the fracture is 16.5 MPa. When the hydraulic fracture

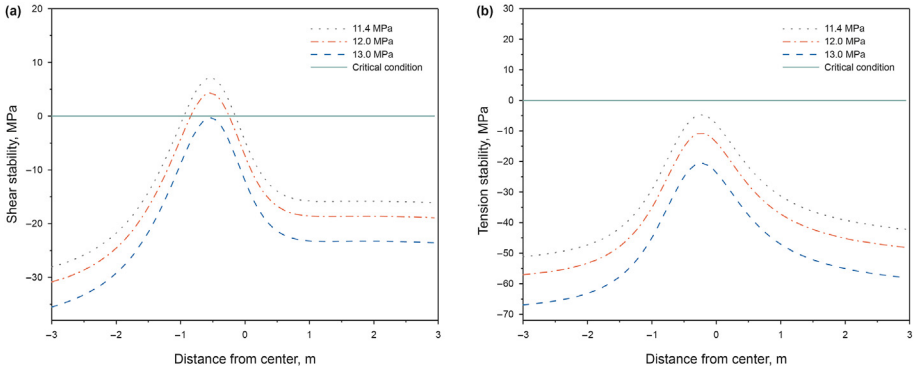

Fig. 15. (**a**) Effect of horizontal stress difference on shear stability of natural fractures; (**b**) Effect of horizontal stress difference on the tension stability of natural fractures.

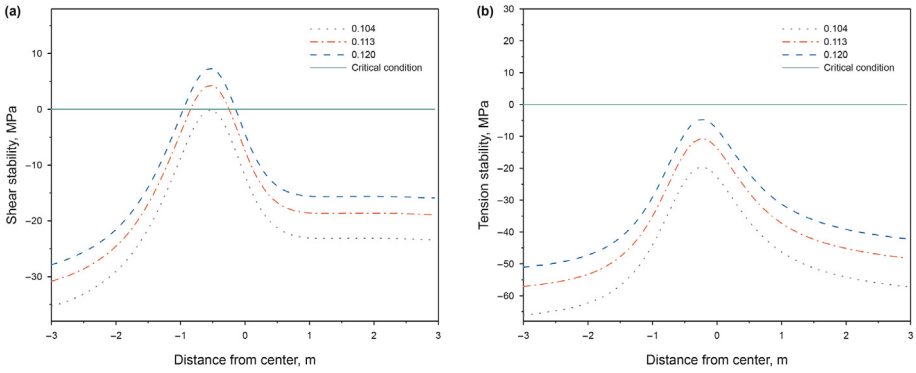

Fig. 16. (**a**) Effect of horizontal stress difference coefficient on shear stability of natural fractures; (**b**) Effect of horizontal stress difference factor on the tension stability of natural fractures.

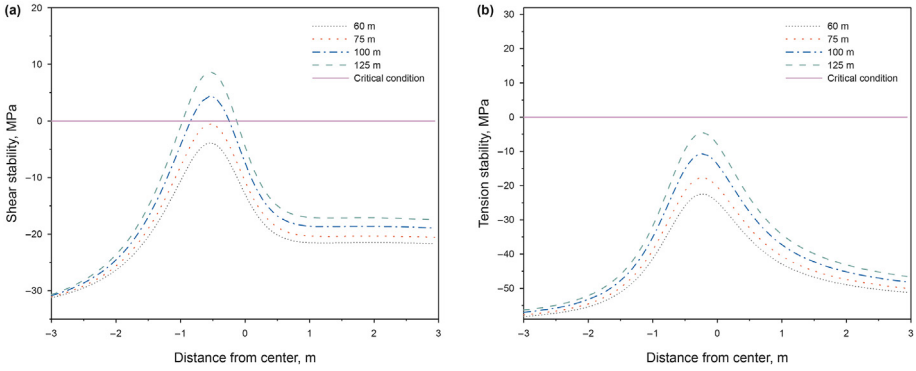

Fig. 17. (**a**) Effect of hydraulic fracture half length on shear stability of natural fractures; (**b**) Effect of hydraulic fracture half length on natural fracture tension stability.

Table 2
Fracture development around the well perimeter in layer 150–155 of Well X.

Well section	Physical analysis of natural fracture development			
	Analytical direction	Number of natural fractures	Fracture orientation	Fracture alignment
5390–5440	East	4	30	NNE
	120°	7	30	NNE
	West	5	0	SN
	300°	4	0	SN

Table 3
Initial parameters of natural fracture stability analysis of No. 150–155 layer.

Influencing factors	Parameter values	Influencing factors	Parameter values
Maximum horizontal principal stress	122 MPa	Minimum horizontal principal stress	110 MPa
Vertical principal stress	137 MPa	Poisson ratio	0.2
Inherent shear strength of natural fractures	7 MPa	Pore pressure	66 MPa
Degree of natural fracture closure	0.9	Hydraulic fracture half slit length	60 m
Friction coefficient in natural fracture	0.6	Net pressure	\
Approach angle	\	Approaching distance	1.5 m

has passed through the natural fracture, let the tip of the hydraulic fracture be 1.5 m away from the natural fracture at this time, the following results are obtained by the fracture stability model calculation.

In the case of a north-south fracture (azimuth 0°), when the hydraulic fracture does not pass through the natural fracture, the natural fracture is destabilized by a net pressure of 16.5 MPa in the fracture. However, when the hydraulic fracture crosses the natural fracture, the natural fracture does not enter a state of instability under the same net pressure (16.5 MPa).

If the hydraulic fracture has passed through the natural fracture, the stability of NF is shown in Fig. 21. The critical shear destabilization net pressure condition is reached when the net pressure in the hydraulic fracture seam reaches 21.1 MPa. When the net pressure reaches 29.5 MPa, the wellhead pressure reaches 73.5 MPa, at which point the natural fracture is activated to an increased extent and nearly half of the length of the natural fracture enters a destabilized state. That is, the natural fracture is activated only after

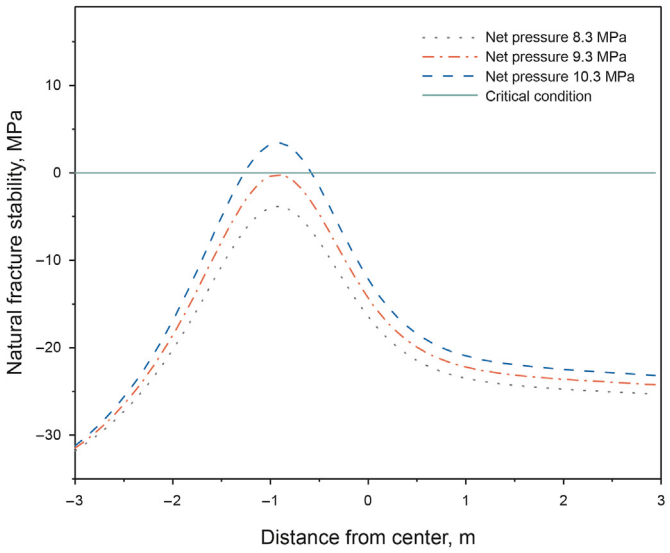

Fig. 18. Determination of fracture stability at an azimuth of 30°.

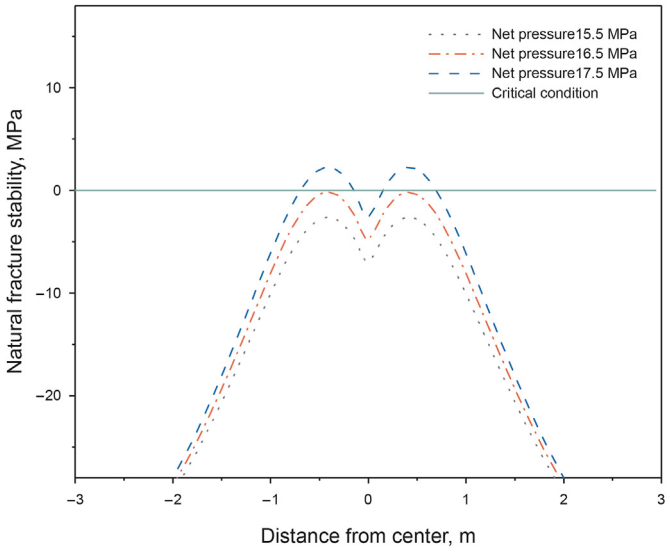

Fig. 19. Determination of fracture stability at an azimuth of 0°.

the net pressure rises by 5–13 MPa.

In the X well hydraulic fracturing, the long fractures were firstly created by using high viscosity fluids together with the pre-acid to communicate as many natural fracture zones as possible. This step is to make full use of the permeability of NF. Then, temporary plugging and higher displacement slick water are employed to open and fill the natural fractures near the well. After the natural fractures near the well are opened and filled, temporary plugging and high displacement slicker water are employed again to further increase the net pressure in the fractures and therefore create a complex fracture. In the third step, the main fracture is filled and the seam opening is supported to ensure permeability of the main fracture and the seam opening.

The construction pressure curve and discharge displacement curve for hydraulic fracturing of Well X is plotted in Fig. 22. It can be seen that before the first temporary plugging, the construction pressure was around 65 MPa. After the temporary plugging, the construction pressure gradually increased to 85 MPa and then a

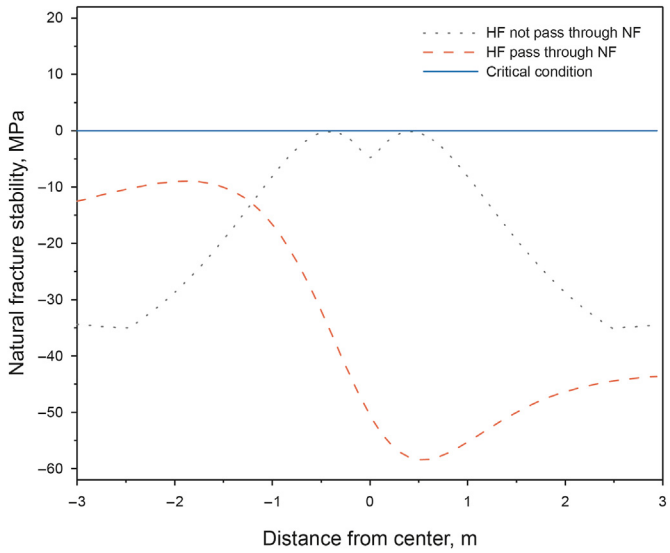

Fig. 20. Stability of hydraulic fractures through/without natural fractures at net pressure of 16.5 MPa.

drop in the pressure occurred after maintaining a period of high pressure. The pressure drop indicates that the fracturing fluid entered the natural fractures and the natural fractures were activated to form a fracture network together with the hydraulic fractures.

In summary, when developing reservoirs where the orientation of natural fracture is approximately orthogonal to the orientation of maximum principal stress, orientation of the horizontal borehole can be parallel to the orientation of natural fracture, followed by high volume fracturing to make the hydraulic fractures communicate with multiple natural fractures as shown in Fig. 23. The natural fractures are activated by raising the net hydraulic fracture pressure through temporary plugging, so that they act as hydraulic fracture branch joints and together form a fracture network. In subsequent developments, the fracturing process can be further adjusted to increase the complexity of the seam network and enhance the extraction effect.

5. Conclusions

Through the formulation of the analytical stability model, extensive parametric studies and analysis of field data, this study investigates the factors influencing the stability of natural fractures and proposes an optimization scheme for borehole trajectories and hydraulic fracturing in the investigated block. The main conclusions of this study are as follows.

(1) A natural fracture stability model based on the Mohr-Coulomb rupture criterion was developed. When a hydraulic fracture approaches a natural fracture, the natural fracture is affected by both the original *in-situ* stress field and the hydraulic fracturing-induced stress field. Natural fractures are more susceptible to shear slip rather than tension damage.

(2) The factors influencing the stability of natural fractures are analyzed. The stability of natural fractures is affected by the approach distance and approach angle between hydraulic fractures and natural fractures, as well as the difference in principal *in-situ* stress, stress difference coefficient, net hydraulic fracture pressure and pore pressure of the formation. The smaller the approach distance, the smaller the approach

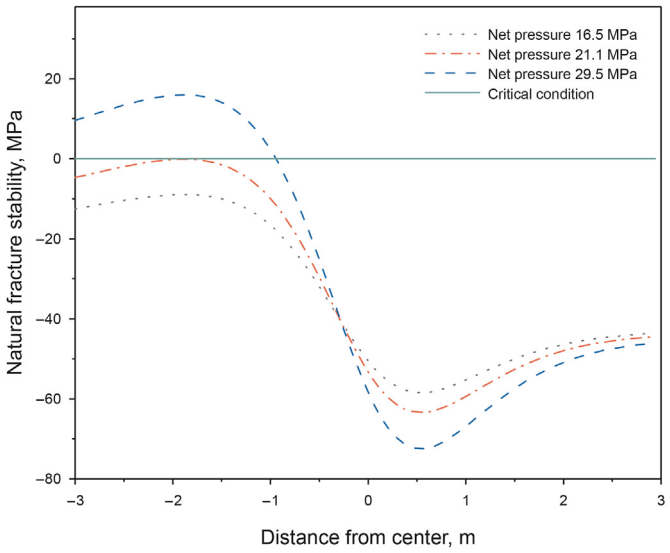

Fig. 21. Natural fracture destabilization under different net pressure conditions after the hydraulic fracture crosses the natural fracture.

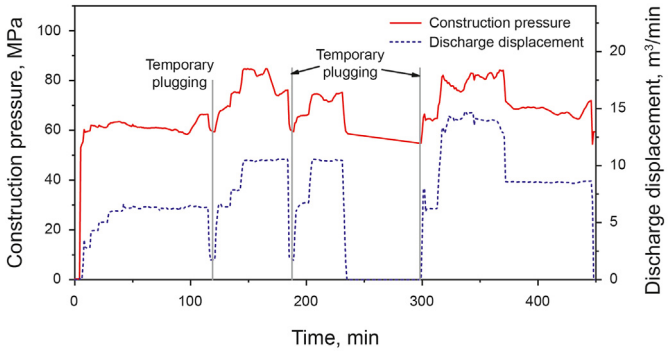

Fig. 22. Fracturing construction curve in Well X.

angle, the smaller the horizontal stress difference, the larger the horizontal stress difference coefficient, the higher the net hydraulic fracture pressure, the higher the formation pore pressure and the longer the hydraulic fracture, the more likely the natural fracture will become unstable.

(3) The validity of the fracture stability model was verified. In the hydraulic fracturing process of Well X, the hydraulic fracture was first made to pass through the natural fracture by using large displacement of slick water, and then the net pressure inside the hydraulic fracture was increased by temporary plugging. When the wellhead pressure reached around 85 MPa, the natural fracture was activated, which matched well with the theoretical results of the fracture stability model and proved the validity of the model.

(4) The induced stress field generated by a hydraulic fracture that already passed through natural fracture acts as an inhibitor to the activation of the natural fracture. The natural fractures can be activated by increasing the net pressure in the seam through temporary plugging. For the situation where there are a large number of natural fractures orthogonal to the direction of the maximum principal stress in the Changling block of the Songliao Basin, hydraulic fractures can be used to connect a large number of natural fractures, and then activate the natural fractures by increasing the net pressure after using them as branching fractures to form a complex fracture network and improve the extraction effect.

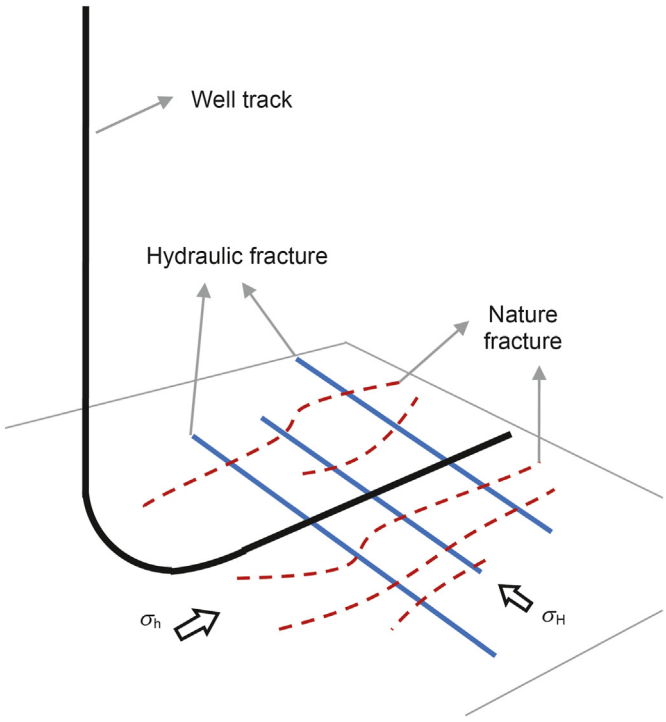

Fig. 23. The strike of natural fractures is orthogonal to the maximum principal stress, and hydraulic fractures communicate with natural fractures to form fracture networks.

Declaration of competing interest

The authors declare that they have no known competing financial interests or personal relationships that could have appeared to influence the work reported in this paper.

Acknowledgments

This work was funded by the subprojects of the National Key R&D Program of China (2020YFA0710600) and the NSFC (National Natural Science Foundation of China, grant 42374132).

References

Altammar, M.J., Agrawal, S., Sharma, M.M., 2017. Effect of Geological Layer Properties on Hydraulic-Fracture Initiation and Propagation: an Experimental Study. SPE Hydraulic Fracturing Technology Conference and Exhibition, Texas, USA. https://doi.org/10.2118/184871-MS.

Blanton, T.L., 1986. Propagation of hydraulically and dynamically induced fractures in naturally fractured reservoirs. SPE Unconventional Gas Technology Symposium, Louisville, Kentucky. https://doi.org/10.2118/15261-MS.

Bunger, A.P., Kear, J., Jeffrey, R.G., Prioul, R., Chuprakov, D., 2015. Laboratory Investigation of Hydraulic Fracture Growth Through Weak Discontinuities with Active Ultrasound Monitoring. In: ISRM 13th International Congress on Rock Mechanics, Canada.

Chen, H.H., Yang, C.Y., Li, J.P., Sun, D.A., 2021. A general method to incorporate three-dimensional cross-anisotropy to failure criterion of geomaterial. Int. J. GeoMech. 21 (12), 04021241. https://doi.org/10.1061/(ASCE)GM.1943-5622.0002224.

Chi, A., Li, X.X., Zhang, J., Jia, D., Tan, W.J., 2018. Experimental investigation of propagation mechanisms and fracture morphology for coalbed methane reservoirs. Petrol. Sci. 15 (4), 815–829. https://doi.org/10.1007/s12182-018-0252-z.

Chuprakov, D.A., Zhubayev, A.S., 2010. A variational approach to analyze a natural fault with hydraulic fracture based on the strain energy density criterion. Theor. Appl. Fract. Mech. 53 (3), 221–232. https://doi.org/10.1016/j.tafmec.2010.06.007.

Dong, K., Liu, N.Z., Chen, Z.W., Huang, R., Ding, J.H., Niu, G., 2019. Geomechanical

analysis on casing deformation in Longmaxi shale formation. J. Pet. Sci. Eng. 177, 724–733. https://doi.org/10.1016/j.petrol.2019.02.068.
Dyer, R., 1988. Using joint interactions to estimate paleostress ratios. J. Struct. Geol. 10 (7), 685–699. https://doi.org/10.1016/0191-8141(88)90076-4.
Gong, W.B., Yang, C.Y., Li, J.P., Xu, L.C., 2021. Undrained cylindrical cavity expansion in modified cam-clay soil: a semi-analytical solution considering biaxial in-situ stresses. Comput. Geotech. 130, 103888. https://doi.org/10.1016/j.compgeo.2020.103888.
Guo, Y.T., Yang, C.H., Jia, C.G., Xu, J.B., Wang, L., Li, D., 2014. Research on hydraulic fracturing physical simulation of shale and fracture characterization methods. Chin. J. Rock Mech. Eng. 33 (1), 52–59. https://doi.org/10.13722/j.cnki.jrme.2014.01.006 (in Chinese).
Huang, L.K., Dontsov, E., Fu, H.F., Lei, Y., Weng, D.W., Zhang, F.S., 2022. Hydraulic fracture height growth in layered rocks: perspective from DEM simulation of different propagation regimes. Int. J. Solid Struct. 238, 111395. https://doi.org/10.1016/j.ijsolstr.2021.111395.
Jeffrey, R.G., Weber, C.R., 1994. In: Hydraulic Fracturing Experiments in the Great Northern Coal Seam. SPE Asia Pacific Oil and Gas Conference, Melbourne, Australia. https://doi.org/10.2118/28779-MS.
Lei, Q., Weng, D.W., Xiong, S.C., Liu, H.B., Guan, B.S., Deng, Q., Yan, X.M., Liang, H.B., Ma, Z.Y., 2021. Progress and development directions of shale oil reservoir stimulation technology of China National Petroleum Corporation. Petrol. Explor. Dev. 48 (5), 1198–1207. https://doi.org/10.1016/S1876-3804(21)60102-7.
Lei, Q., Xu, Y., Cai, B., Guan, B.S., Wang, X., Bi, G.Q., Li, H., Li, S., Ding, B., Fu, H.F., Tong, Z., Li, T., Zhang, H.Y., 2022a. Progress and prospects of horizontal well fracturing technology for shale oil and gas reservoirs. Petrol. Explor. Dev. 49 (1), 191–199. https://doi.org/10.1016/S1876-3804(22)60015-6.
Lei, Q., Yang, Z.W., Weng, D.W., Liu, H.T., Guan, B.S., Cai, B., Fu, H.F., Liu, Z.L., Duan, Y.Y., Liang, T.C., Ma, Z.Y., 2022b. Techniques for improving fracture-controlled stimulated reservoir volume in ultra-deep fractured tight reservoirs: a case study of Kuqa piedmont clastic reservoir, Tarim Basin, NW China. Petrol. Explor. Dev. 49 (5), 1169–1184. https://doi.org/10.11698/PED.20210674.
Li, J., Guo, B.Y., Feng, Y., 2014. An analytical solution of fracture-induced stress and its application in shale gas exploitation. J. Energy Resour. Technol. 136 (2), 023102.1–023102.6. https://doi.org/10.1115/1.4025714.
Liu, X.Q., Qu, Z.Q., Guo, T.K., Sun, Y., Wang, Z.Y., Bakhshi, E., 2019. Numerical simulation of non-planar fracture propagation in multi-cluster fracturing with natural fractures based on Lattice methods. Eng. Fract. Mech. 220, 106625. https://doi.org/10.1016/j.engfracmech.2019.106625.
Lu, Q.L., Liu, Z., Guo, J.C., He, L., Li, Y.C., Zeng, J., Ren, S., 2021. Hydraulic fracturing induced casing shear deformation and a prediction model of casing deformation. Petrol. Explor. Dev. 48 (2), 460–468. https://doi.org/10.1016/S1876-3804(21)60037-X.
Maxwell, S.C., 2011. What does microseismicity tells us about hydraulic fractures? SEG Tech. Progr. Expand. Abstr. 1565–1569. https://doi.org/10.1190/1.3627501.
Meng, H., Ge, H.K., Bai, J., Wang, X.Q., Zhang, J.L., Shen, Y.H., Zhang, Z.D., 2021. Variation of induced stress field during hydraulic fracture closure and its influence on subsequent fracture. Energy Rep. 7, 7785–7803. https://doi.org/10.1016/j.egyr.2021.10.105.
Olson, J.E., Arash, D.T., 2009. Modeling Simultaneous Growth of Multiple Hydraulic Fractures and Their Interaction with Natural Fractures. SPE Hydraulic Fracturing Technology Conference, Texas, USA. https://doi.org/10.2118/119739-MS.
Sesetty, V., Ahmad, G., 2019. In: Simulation and Analysis of Fracture Swarms Observed in the Eagle Ford Field Experiment. SPE Hydraulic Fracturing Technology Conference and Exhibition, Texas, USA. https://doi.org/10.2118/194328-MS.
Shimizu, H., Murata, S., Ishida, T., 2011. The distinct element analysis for hydraulic fracturing in hard rock considering fluid viscosity and particle size distribution. Int. J. Rock Mech. Min. Sci. 48 (5), 712–727. https://doi.org/10.1016/j.ijrmms.2011.04.013.
Sneddon, I.N., 1946. The distribution of stress in the neighbourhood of a crack in an elastic solid. Proc. Roy. Soc. Lond. A. 187 (1009), 229–260. https://doi.org/10.1098/rspa.1946.0077.
Tan, P., Jin, Y., Han, K., Hou, B., Chen, M., Guo, X.F., Gao, J., 2017. Analysis of hydraulic fracture initiation and vertical propagation behavior in laminated shale formation. Fuel 206, 482–493. https://doi.org/10.1016/j.fuel.2017.05.033.
Tan, P., Jin, Y., Yuan, L., Xiong, Z.Y., Hou, B., Chen, M., Wan, L.M., 2019. Understanding hydraulic fracture propagation behavior in tight sandstone–coal interbedded formations: an experimental investigation. Petrol. Sci. 16 (1), 148–160. https://doi.org/10.1007/s12182-018-0297-z.
Tan, P., Pang, H.W., Zhang, R.X., Jin, Y., Zhou, Y.C., Kao, J.W., Fan, M., 2020. Experimental investigation into hydraulic fracture geometry and proppant migration characteristics for southeastern Sichuan deep shale reservoirs. J. Pet. Sci. Eng. 184, 106517. https://doi.org/10.1016/j.petrol.2019.106517.
Tan, P., Jin, Y., Pang, H.W., 2021. Hydraulic fracture vertical propagation behavior in transversely isotropic layered shale formation with transition zone using XFEM-based CZM method. Eng. Fract. Mech. 248, 107707. https://doi.org/10.1016/j.engfracmech.2021.107707.
Tang, J.Z., Wu, K., Li, Y.C., Hu, X.D., Liu, Q.L., Ehlig, C., 2018. Numerical investigation of the interactions between hydraulic fracture and bedding planes with non-orthogonal approach angle. Eng. Fract. Mech. 200, 1–16. https://doi.org/10.1016/j.engfracmech.2018.07.010.
Teufel, L.W., Clark, J.A., 1984. Hydraulic fracture propagation in layered rock: experimental studies of fracture containment. SPE J. 24 (1), 19–32. https://doi.org/10.2118/9878-PA.
Wang, X.Q., Ge, H.K., Han, P., 2018. A new model for fracability evaluation with consideration of natural cracks. J. Geophys. Eng. 15 (4), 1492–1505. https://doi.org/10.1088/1742-2140/aab500.
Wang, X.Q., Xu, J.G., Zhao, C.X., Liu, T.Y., Ge, H.K., Shen, Y.H., Wu, S., Yu, J.Y., Huang, R.Y., 2020. Influence of bedding and mineral composition on mechanical properties and its implication for hydraulic fracturing of shale oil reservoirs. Earthq. Res. China 34 (2), 167–186. https://doi.org/10.19743/j.cnki.0891-4176.202002003.
Wang, X.Q., Ge, H.K., Wang, W.W., Zhang, Q., 2021. Experimental study on stress-related and matrix-related anisotropy in tight reservoirs. Chin. J. Geophys. 64 (12), 4239–4251. https://doi:10.6038/cjg2021P0040 (in Chinese).
Warpinski, N.R., Teufel, L.W., 1987. Influence of geologic discontinuities on hydraulic fracture propagation. J. Petrol. Technol. 39, 209–220. https://doi.org/10.2118/13224-PA.
Weng, X.W., Siebrits, E., 2007. Effect of Production-Induced Stress Field on Refracture Propagation and Pressure Response. SPE Hydraulic Fracturing Technology Conference, Texas, USA. https://doi.org/10.2118/106043-MS.
Yang, C.Y., Gong, W.B., Li, J.P., Gu, X.Y., 2020a. Drained cylindrical cavity expansion in modified Cam-clay soil under biaxial in-situ stresses. Comput. Geotech. 121, 103494. https://doi.org/10.1016/j.compgeo.2020.103494.
Yang, C.Y., Li, L., Li, J.P., 2020b. Service life of reinforced concrete seawalls suffering from chloride attack: theoretical modelling and analysis. Construct. Build. Mater. 263, 120172. https://doi.org/10.1016/j.conbuildmat.2020.120172.
Yang, C.Y., Li, J.P., Li, L., Sun, D.A., 2021. Expansion responses of a cylindrical cavity in overconsolidated unsaturated soils: a semi-analytical elastoplastic solution. Comput. Geotech. 130, 103922. https://doi.org/10.1016/j.compgeo.2020.103922.
Yew, C.H., Weng, X.W., 2015. Mechanics of Hydraulic Fracturing, second ed. https://doi.org/10.1016/C2013-0-12927-3
Yildirim, B., Cao, W.Z., Durucan, S., Korre, A., Wolf, K.H., Bakker, R., Barnhoorn, A., 2018. The Effect of Natural Fracture Heterogeneity on Hydraulic Fracture Performance and Seismic Response in Shale and Coal Formations. 52nd US Rock Mechanics/Geomechanics Symposium, Washington, USA.
Zhang, S.C., Lei, X., Zhou, Y.S., Xu, G.Q., 2015. Numerical simulation of hydraulic fracture propagation in tight oil reservoirs by volumetric fracturing. Petrol. Sci. 12 (4), 674–682. https://doi.org/10.1007/s12182-015-0055-4.
Zhang, L.Q., Zhou, J., Braun, A., Han, Z.H., 2018. Sensitivity analysis on the interaction between hydraulic and natural fractures based on an explicitly coupled hydro-geomechanical model in PFC2D. J. Pet. Sci. Eng. 167, 638–653. https://doi.org/10.1016/j.petrol.2018.04.046.
Zhao, P., Xie, L.Z., Ge, Q., Zhang, Y., Liu, J., He, B., 2020. Numerical study of the effect of natural fractures on shale hydraulic fracturing based on the continuum approach. J. Pet. Sci. Eng. 189, 107038. https://doi.org/10.1016/j.petrol.2020.107038.
Zhao, P., Xie, L.Z., Fan, Z.C., Deng, L., Liu, J., 2021. Mutual interference of layer plane and natural fracture in the failure behavior of shale and the mechanism investigation. Petrol. Sci. 18 (2), 618–640. https://doi.org/10.1007/s12182-020-00510-5.
Zheng, X.Q., Shi, J.F., Cao, G., Yang, N.Y., Cui, M.Y., Jia, D.L., Liu, H., 2022. Progress and prospects of oil and gas production engineering technology in China. Petrol. Explor. Dev. 49 (3), 644–659. https://doi.org/10.1016/S1876-3804(22)60054-5.
Zoback, M.D., Snee, J.L., 2018. Predicted and Observed Shear on Preexisting Faults during Hydraulic Fracture Stimulation. SEG Technical Program Expanded Abstracts, pp. 3588–3592. https://doi.org/10.1190/segam2018-2991018.1.
Zou, Y.S., Zhang, S.C., Ma, X.F., Zhou, T., Zeng, B., 2016. Numerical investigation of hydraulic fracture network propagation in naturally fractured shale formations. J. Struct. Geol. 84, 1–13. https://doi.org/10.1016/j.jsg.2016.01.004.
Zou, Y.S., Gao, B.D., Zhang, S.C., Ma, X.F., Sun, Z.Y., Wang, F., Liu, C.Y., 2022. Multi-fracture nonuniform initiation and vertical propagation behavior in thin interbedded tight sandstone: an experimental study. J. Pet. Sci. Eng. 213, 110417. https://doi.org/10.1016/j.petrol.2022.110417.